scientific reports

Check for updates

OPEN

Method for extracting ship shaft rate features by fusing acoustic and magnetic field

Taotao Xie[1], Qing Ji[1✉], Peng Yu[2✉] & Jiawei Zhang[1]

To address the challenge of detecting small underwater targets, this paper proposes a detection method based on the fusion of acoustic and magnetic fields. The shaft-rate acoustic field and shaft-rate magnetic field of a vessel are both closely related to the rotation of its propeller and contain rich target characteristic information. Using the vessel's shaft-rate information as a key criterion, this paper proposes to fuse the acoustic and magnetic fields to extract the shaft-rate features of the vessel. Specifically, the line spectra of the shaft-rate acoustic and magnetic fields are first extracted using DEMON spectral analysis and power spectral analysis methods, respectively. Subsequently, the extracted line spectra are fused and purified. Finally, the shaft-rate features are extracted based on the greatest common divisor (GCD) method. To verify the effectiveness of the proposed method, real-measured acoustic and magnetic data from multiple vessels were used for experimental validation. The results show that there is a significant frequency correspondence between the line spectra of the shaft-rate acoustic and magnetic fields of the same vessel. By fusing the shaft-rate related line spectra of the acoustic and magnetic fields, the problem of line-spectrum loss in a single physical field, caused by environmental noise and other factors, can be effectively compensated. Moreover, after fusing the acoustic and magnetic fields, the accuracy and stability of the vessel's shaft-rate estimation are significantly better than those of a single physical field, allowing for more reliable extraction of shaft-rate information and enhancing the basis for target identification.

As the world advances in the exploration and development of the ocean, underwater target detection technology has gradually become a focal point of research in both military and civilian sectors. In the military domain, the stealth and high threat level of underwater targets such as submarines and mines make the detection and identification of these targets crucial for national security. This necessitates the development of efficient and accurate detection methods to ensure maritime operational superiority and defensive capabilities.

In the civilian sector, underwater target detection is extensively utilized in various fields including ocean resource exploration, seabed pipeline monitoring, underwater archaeology, and marine environmental monitoring. For instance, in the development of offshore oil and natural gas resources, accurately detecting small underwater targets helps to avoid collision risks during pipeline laying, thus ensuring the smooth progress of resource extraction. Underwater archaeology, on the other hand, relies on dependable detection technologies to discover and locate valuable historical relics like ancient shipwrecks.

The acoustic field is the most intuitive and characteristic physical field of underwater targets, capable of reflecting features such as radiated noise, propeller noise, and cavitation noise[1]. As a traditional underwater detection technology, acoustic detection utilizes the propagation characteristics of sound waves in water to achieve target detection[2]. However, the complexity of the marine environment, including variations in sound velocity, multipath propagation, the influence of seabed topography, and marine biological noise, severely restricts the performance of acoustic detection[3]. The speed of sound changes with fluctuations in seawater temperature, salinity, and depth, causing the path of sound waves to bend and reducing the accuracy of target positioning[4–6]. Multipath propagation can create echoes in the received signals[7,8], interfering with the identification of target signals. This issue is particularly pronounced in complex maritime areas such as shallow waters[9], severely impacting the detection capabilities for small targets.

Magnetic field detection is based on the magnetic field anomalies caused by underwater targets to achieve target detection[10,11] and is commonly used in aerial magnetic surveys[12] and underwater target detection[13].

[1]Naval University of Engineering, Wuhan, China. [2]Naval Petty Officer Academy, Bengbu, China. ✉email: jiumingya886@163.com; 15527176227@163.com

However, various natural and man-made sources of magnetic interference exist in the ocean[14], such as variations in the Earth's magnetic field, electromagnetic noise in the ocean, and interference from other magnetic objects[15]. Marine biological activities also generate electromagnetic fields[16], which can have a certain impact on the ambient magnetic field. These interferences can mask the weak magnetic signals produced by small underwater targets, increasing the difficulty of magnetic detection. Moreover, the magnetic characteristics of different types of small underwater targets are relatively similar, making it difficult to accurately distinguish the type and nature of the targets based solely on magnetic information. This limitation restricts the application scope of magnetic field detection[17,18].

The theory of information fusion initially originated in underwater signal processing. In 1973, American researchers used multiple independent continuous sonar signals to detect enemy underwater targets[19]. The results indicated that the performance of multiple continuous sonar systems was superior to that of a single sonar system. Consequently, underwater environments have become one of the most critical subjects of study in multi-signal fusion technology[20–22].In the realm of underwater electromagnetic detection systems, the use of magnetic signals dates back to World War II with the deployment of magnetic detonators. During the 1950 s, the Soviet Union equipped itself with non-contact electric field detonation mines. In the early 1960 s, the United States and Canada utilized ice floes to set up electric field detection electrodes, complemented by satellite positioning systems to search for Soviet submarines[23].By the late 1960 s, the Soviet Union had successfully developed an electromagnetic sea denial control system[24].In the late 1970 s, the United States conducted measurements of the electromagnetic fields associated with the shaft frequency of naval vessels. By employing matched filtering techniques, they were able to enhance the detection range, achieving the longest detection distance of up to 1.6 km. This demonstrated the feasibility of using shaft-rate electric fields for long-range detection and also proposed the use of time-harmonic electric dipoles as a field source model for the electric fields of ships[25].In the early 1980 s, the United States utilized an electric field detection system to detect signals from distant current sources, while the Soviet Union developed an underwater early warning system. After the 1990 s, underwater low-frequency electromagnetic detection technology saw new advancements, with countries such as the United States and Germany researching the shaft frequency magnetic fields generated by the residual magnetism of submarine propellers[26].

Entering the twenty-first century, with the advancement of electromagnetic field detection technology and sensors[27], the United Kingdom, Spain, and France have developed multi-physical field maritime surveillance systems. The United States has been actively working on the development of underwater electromagnetic detection buoys. Both Russia and Ukraine have been intensifying their research into the detection of underwater electric field targets. Researchers in Sweden have indicated that low-frequency electric field signals (0.3–3000 Hz) can be detected over several kilometers in shallow water environments[28].The demand for oceanic information fusion is growing day by day in various fields such as maritime safety supervision, emergency response to maritime incidents, search and rescue operations at sea[29], marine environmental monitoring and protection[30], ocean resource exploration and development, and marine disaster prevention and mitigation. In the military domain, oceanic information fusion is the most crucial core support technology for maritime military information systems[31].

When sound waves propagate in seawater, multi-path effects formed by reflections from the water surface and seabed cause line spectrum missing reports or false frequency points, affecting the accuracy of shaft frequency extraction. With the rapid development of ship vibration and noise reduction technologies, marine background noise (such as waves and biological activities) overlaps with ship radiated noise in the low-frequency band, making weak signals from small targets prone to being masked. Along with the advancement of ship degaussing and de-energizing technologies, ship magnetic field signals have been significantly reduced. Moreover, the magnetic field intensity decays inversely with the square of distance, resulting in low detection sensitivity for small targets at long ranges—making single magnetic field signals difficult to uniquely characterize the target. From this, it is evident that using a single physical field for target detection, identification, positioning, and monitoring cannot meet practical requirements[32]. Both acoustic and magnetic fields have their respective advantages when detecting underwater targets, but a single signal often fails to fully reflect the characteristics of the target[33]. To overcome the limitations of single acoustic or magnetic field detection, underwater target detection technology that integrates both acoustic and magnetic fields has emerged[34]. By leveraging the complementary information from acoustic and magnetic signals, a more comprehensive acquisition of the features of underwater targets can be achieved, enhancing the accuracy and reliability of detection[35,36]. Through integrated analysis, the impact of marine environmental interference on detection results can be effectively reduced, strengthening the ability to discern targets, and thus enabling efficient detection and identification of small underwater targets in complex marine environments[37].

Shaft-rate acoustic field and magnetic field analysis
Shaft-rate acoustic field
During navigation, ships generate a variety of noises that collectively form the radiated noise field of the vessel. The radiated noise from ships primarily consists of mechanical noise, propeller noise, and hydrodynamic noise. Among these, propeller noise stands out as a significant component of the ship's radiated noise. Its generation mechanism is closely related to factors such as the rotation of the propeller and cavitation.

During the rotation of a ship's propeller, the blades interact dynamically with the water, generating periodic pressure fluctuations that emit acoustic noise. Concurrently, as the rotational speed of the propeller escalates, cavitation phenomena occur when the local water pressure falls below the vapor pressure of water at saturation. The inception, evolution, and implosion of cavitation bubbles significantly augment the acoustic emission. These noises are characterized by pronounced periodicity, with their spectral components encompassing the shaft

frequency associated with the propeller's rotation, as well as its harmonic multiples. A simplified time-domain simulation model for ship radiated noise is as follows[38]:

$$x(t) = [1 + a(t)] g_c(t) + g_l(t) \tag{1}$$

In this model:

$x(t)$ represents the total radiated noise signal observed at time t.

$g_l(t)$ is the periodic component associated with the propeller rotation, often including the shaft frequency and its harmonics.

$g_c(t)$ denotes the broadband noise component, primarily related to cavitation caused by the propeller.

$a(t)$ is a modulation signal indicating the periodic modulation effects caused by the propeller's rotation.

The shaft-rate line spectrum can typically be expressed as specific frequency components related to the number of propeller blades and the rotational speed. Specifically, the shaft frequency refers to the fundamental frequency of the propeller rotation, and the line spectrum refers to the discrete frequency lines in the frequency domain. For a ship's propeller, the shaft-rate line spectrum can be expressed as:

$$f_m = m \cdot n \cdot s \tag{2}$$

where:

f_m is the frequency of the m-th harmonic;

n is the number of propeller blades;

s is the shaft frequency of the propeller, measured in Hz.

In practical applications, the shaft-rate line spectrum includes not only the fundamental frequency but also its harmonic frequencies, which can reveal the rotation state and characteristics of the propeller. Analysis of these frequency components allows for target identification, classification, and monitoring of the propeller's operating condition.

Shaft-rate magnetic field

As a submersible magnetic target, a ship exhibits complex magnetic field characteristics. During its construction, the extensive use of ferromagnetic materials leads to magnetization by the Earth's magnetic field, resulting in residual magnetism. The very-low-frequency (VLF) electromagnetic field, typically in the range of 1–7 Hz, is generated by the relative motion between the ship's propeller, bearings, and hull circuits. When the propeller rotates, irregularities in the bearings produce periodic currents, thereby generating an electromagnetic field with a frequency matching that of the propeller's rotation[39]. Additionally, the rotation of the magnetic axis also induces an axis-frequency magnetic field, which can be reliably detected using fluxgate sensors[40], the mechanism of axis-frequency magnetic field generation is illustrated in Fig. 1. This type of magnetic field propagates slowly in the seawater environment and attenuates gradually, thus enabling a longer detection range. As a result, it is widely employed for the reconnaissance and localization of underwater targets.
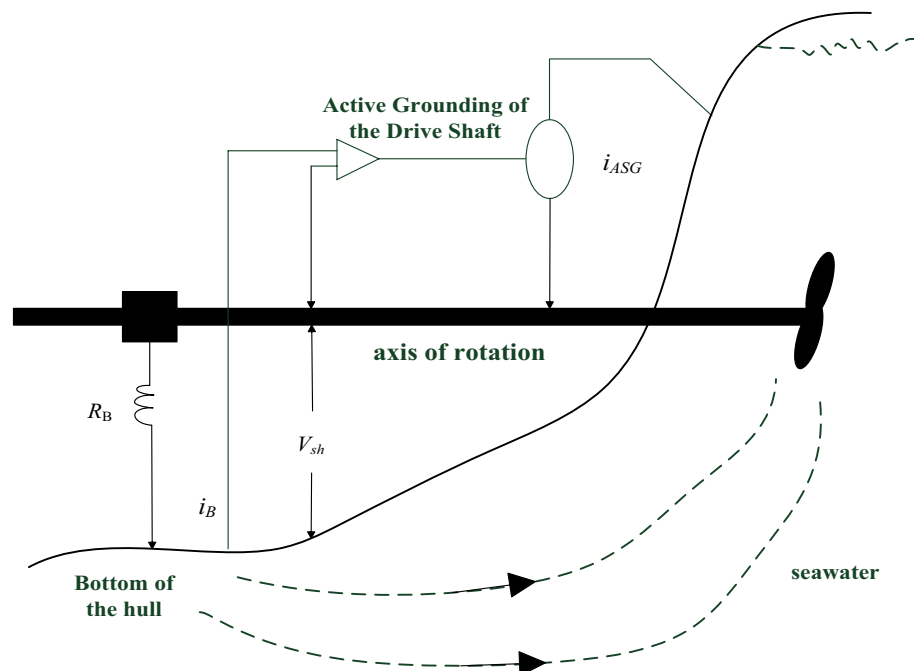
Fig. 1. Mechanism of shaft frequency signal generation.

In the modeling of the magnetic fields of small underwater targets, when the length of a wire current source is less than approximately five times the distance from its center to the observation point, the target can be effectively approximated as a magnetic dipole[41]. This approximation is valid because, at a considerable distance, the magnetic field distribution of the target is predominantly determined by its magnetic moment, and the magnetic dipole model aptly characterizes the magnetic field properties at such distances.

The mathematical model of the magnetic field generated by a dipole can be expressed as:

$$B(r) = \frac{\mu_0}{4\pi}\left[\frac{3(m \cdot r)r}{r^5} - \frac{m}{r^3}\right] \tag{3}$$

In the equation, $B(r)$ represents the magnetic flux density at a spatial point r, μ_0 is the permeability of free space, m denotes the magnetic moment of the target, and r is the distance from the observation point to the center of the magnetic dipole.

In the model, the magnetic moment (m) is a crucial parameter that mirrors the magnetic properties of the target, which are influenced by factors such as the material, shape, and magnetization state of the target. The intensity of the magnetic field B is not only related to the magnitude of the target's magnetic moment but also closely associated with the distance r and orientation of the observation point relative to the target. As the distance r increases, the magnetic field strength diminishes rapidly, demonstrating an inversely proportional relationship with respect to the distance r^3.

In the context of seabed exploration scenarios, a stratified model consisting of air, seawater, and seabed layers is established, the specific model is shown in Fig. 2. The medium is assumed to be homogeneous and isotropic linear. The coordinate plane *XOY* coincides with the interface between air and seawater, and the Z-axis is directed vertically downward. The target source is located within the seawater layer at a certain depth z', meaning the source center coordinates are (x',y',z'). Consequently, the magnetic vector potential **A** satisfies the following equations in the air, seawater, and seabed layers:

$$\nabla^2 A_0 y + k_0^2 A_0 y = 0, z < 0 \tag{4}$$

$$\nabla^2 A_1 y + k_1^2 A_1 y = -\mu_0 P\delta(x)\delta(y)\delta(z - z') \quad 0 < z < d \tag{5}$$

$$\nabla^2 A_2 y + k_2^2 A_2 y = 0, z > d \tag{6}$$

$$\nabla^2 A_0 z + k_0^2 A_0 z = 0, z < 0 \tag{7}$$
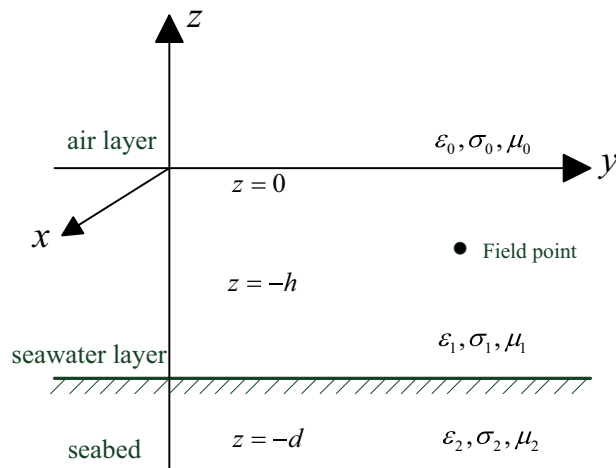
$$\nabla^2 A_1 z + k_1^2 A_1 z = 0, 0 < z < d \tag{8}$$

$$\nabla^2 A_2 z + k_2^2 A_2 z = 0, z > d \tag{9}$$

$$A_{0y}\big|_{z=0} = A_{1y}\big|_{z=0} \tag{10}$$

$$A_{1y}\big|_{z=d} = A_{2y}\big|_{z=0} \tag{11}$$

$$A_{0z}\big|_{z=0} = A_{1z}\big|_{z=0} \tag{12}$$

$$A_{1z}\big|_{z=d} = A_{2z}\big|_{z=d} \tag{13}$$

$$\frac{\partial A_{0y}}{\partial z}\bigg|_{z=0} = \frac{\partial A_{1y}}{\partial z}\bigg|_{z=0} \tag{14}$$

Fig. 2. Schematic diagram of air-seawater-seafloor electromagnetic field modeling.

$$\left.\frac{\partial A_{1y}}{\partial z}\right|_{z=d} = \left.\frac{\partial A_{2y}}{\partial z}\right|_{z=d} \tag{15}$$

$$\left.\frac{\partial A_{0y}}{\partial y}\right|_{z=0} = \left.\frac{\partial A_{0z}}{\partial z}\right|_{z=0} \tag{16}$$

$$\rho_1\left(\frac{\partial A_{1y}}{\partial y} + \frac{\partial A_{1z}}{\partial z}\right)\Bigg|_{z=d} = \rho_2\left(\frac{\partial A_{2y}}{\partial y} + \frac{\partial A_{2z}}{\partial z}\right)\Bigg|_{z=d} \tag{17}$$

In all the above equations:

$\mathbf{A}_0$, $\mathbf{A}_1$, and $\mathbf{A}_2$ represent the magnetic vector potentials in the air layer, seawater layer, and seabed layer, respectively;

The subscripts y and z denote the components in the two respective directions;

k_0, k_1, and k_2 are the complex wave numbers in the air layer, seawater layer, and seabed layer, respectively;

$\mathbf{P}$ represents the electric dipole moment;

μ_0 is the permeability of free space;

ρ_1 is the resistivity of seawater, and ρ_2 is the resistivity of the seabed;

z is the depth of the measurement point (i.e., the depth of the receiver);

d is the thickness of the seawater layer.

Using the integral equation method to solve the above equations allows us to obtain the shaft-rate electric and magnetic fields generated by the target at different positions within the seawater[42].

Shaft-rate frequency feature extraction method integrating acoustic field and magnetic field

Simultaneous acquisition of shaft frequency information from both acoustic and magnetic fields enhances the identification and assessment of the target. This is because acoustic and magnetic signals reflect the characteristics of the ship target from different physical perspectives and exhibit complementary properties. Acoustic signals primarily capture the pressure fluctuations generated by the ship's motion through water, while magnetic signals mainly reflect the ship's magnetic features. By integrating the shaft frequency information from these two types of signals, a more comprehensive understanding of the ship target's status can be achieved.

To extract the shaft frequency information from the acoustic field of a ship target, it is necessary to carry out noise reduction and filtering processing on the original signal[43,44]. The DEMON (Detection of Envelope Modulation On Noise) analysis method is commonly employed. The fundamental principle of this method is based on the amplitude modulation phenomenon present in the radiated noise of ships. Due to the rotation of the propeller, its shaft frequency and blade frequency can cause amplitude modulation in the ship's radiated noise. The modulation frequency is equal to either the propeller's rotational speed (shaft frequency) or the blade passing frequency (shaft frequency multiplied by the number of blades). For the magnetic field, power spectral density estimation is directly employed to eliminate the continuous spectrum and thereby obtain the line spectrum. Subsequently, the line spectra extracted from the acoustic and magnetic fields are fused at the data level and subjected to line spectrum purification. Finally, the shaft frequency is extracted using the Greatest Common Divisor (GCD) method.

Line spectrum extraction

1. Acoustic line spectrum extraction

Step 1: Apply a bandpass filter to the input signal, followed by squaring to obtain the envelope signal. Perform an FFT on the envelope signal to generate the DEMON spectrum. Shift the DEMON spectrum positively to ensure its minimum value is 0 dB.

Step 2: Given that the acoustic sampling rate is significantly higher than the magnetic field sampling rate and the shaft frequency is relatively low, apply a 50 Hz low-pass filter to the DEMON spectrum. Alternatively, down-sampling can be employed.

Step 3: Use a sliding window fitting method to obtain the continuous spectrum from the DEMON spectrum. Multiply this continuous spectrum by a coefficient κ_1 to establish a threshold η_1. Identify the stronger line spectra that exceed this threshold η_1. To mitigate the influence of these stronger line spectra on the continuous spectrum obtained via the sliding window fitting, remove them from the DEMON spectrum obtained in Step 2. Then, reapply the sliding window fitting method to obtain the continuous spectrum. Multiply this continuous spectrum by another coefficient κ_2 (where $\kappa_1 > \kappa_2$; the first threshold κ_1 is used to extract and remove"strong line spectra", avoiding their interference with continuous spectrum fitting. The second threshold $\kappa_1 > \kappa_2$ is applied to extract"medium-intensity line spectra"from the remaining signals, ensuring completeness.) to establish the final threshold η_2. Calculate the line spectra in the DEMON spectrum obtained in Step 2 that exceed this threshold η_2.

Step 4: Determine the peak values of the extracted line spectra (i.e., the difference between the peak and the average of the adjacent troughs on either side). Set a fixed threshold η_3, which is specified as $\eta_3 = 8 \sim 10$ dB in this study. Remove the line spectra obtained in Step 3 that exceed this fixed threshold η_3. The remaining line spectra constitute the acoustic line spectrum.

In the signal processing, non-target factors such as environmental noise and equipment interference may generate pseudo-peaks (false line spectra) in the frequency spectrum. However, the real line spectrum

signals of ship targets, such as shaft frequency and blade frequency, due to the modulation effect generated by physical processes such as propeller rotation, their peak intensities are usually higher than the background noise. According to the ship physical field, if the threshold is too high (> 10 dB), it may filter out some weak but real line spectra (such as long-distance target signals or low-frequency modulation components), leading to information loss; if the threshold is too low (< 8 dB), it may retain more noise pseudo-peaks, affecting the accuracy of subsequent shaft frequency extraction. Therefore, a threshold of 8–10 dB can effectively distinguish real signals from random noise, ensuring that the extracted line spectra correspond to the real vibration or modulation characteristics of the target.

2. Magnetic line spectrum extraction

In the extraction of magnetic field line spectra, envelope detection is unnecessary. Instead, the process directly involves estimating the power spectral density of the input signal, followed by line spectrum extraction as described in Steps 3 and 4.

Line spectrum fusion and purification

Given that the line spectra of the acoustic and magnetic fields have only been positively shifted (to set the minimum value to 0 dB) without undergoing normalization, their relative intensities are retained. Therefore, the line spectra extracted from the acoustic and magnetic fields are directly combined, sorted in ascending order of frequency, and then purified to merge line spectra with similar frequencies.

During the analysis of extensive measured data, it has been observed that multiple line spectra may occur near the same frequency point. However, these spectra actually correspond to the same frequency and should be merged. Considering that the shaft frequency (corresponding to the propeller rotation rate) of medium and large-sized vessels typically ranges from 1 to 7 Hz, to ensure the accuracy of the extracted line spectra, line spectra with differences less than 1 Hz are merged into a single line spectrum. Specifically, only the line spectrum with the highest amplitude among those with differences less than 1 Hz is retained. By the end of this step, the line spectral features related to the ship's shaft frequency are essentially obtained. Since these line spectral features integrate acoustic and magnetic field data with a certain signal-to-noise ratio, the merged line spectra are comprehensive and can serve as a spectral feature set for target identification.

Shaft frequency extraction using the greatest common divisor (GCD) method

The acoustic line spectrum may suffer from missed reports due to multi-path interference, potentially causing the loss of partial line spectra or the generation of several false spectral frequency points. Therefore, the minimum value in the acoustic line spectrum does not necessarily correspond to the shaft frequency, and the greatest common divisor (GCD) method is generally used for shaft frequency extraction. For magnetic field signals, although they are not affected by multi-path interference, practical measurements have shown that the shaft frequency does not necessarily correspond to the maximum amplitude in the line spectrum sequence.

In the shaft frequency extraction of ship targets, the GCD method analyzes the frequency relationship of the line spectrum sequence to extract the fundamental frequency (shaft frequency) that can divide most line spectrum frequencies. Its core lies in leveraging the physical characteristic that"the shaft frequency and blade frequency (shaft frequency × number of blades) have an integer multiple relationship,"bypassing signal distortion or amplitude interference to deduce the fundamental frequency from the frequency logic of the line spectrum. This method exhibits strong robustness against issues such as multi-path interference in acoustic fields and non-maximum amplitudes in magnetic fields. Meanwhile, by fusing the difference frequency statistics and quality factor screening of signals, it achieves accurate shaft frequency extraction, serving as an effective strategy for feature recognition of ship targets. The specific solution steps are as follows:

1) Difference frequency calculation.

Compute the difference frequencies $f_{i,j}$:
$f_{i,j} = f_i - f_j, i, j = 1, 2, \cdots, M; i > j$ among the line spectra in the combined acoustic and magnetic field sequence $\boldsymbol{F}_m = [f_1,\ f_2, \cdots,\ f_m]$.

In the formula, M represents the number of line spectra in $\boldsymbol{F}_m$. Subsequently, the difference frequencies are sorted in ascending order to form the difference frequency array $\boldsymbol{F}_{i,j}$.

2) Quality factor calculation.

Step 1: To solve for the number of identical or similar elements in $\boldsymbol{F}_{i,j}$, set a frequency difference Δf_1. If the frequency difference between k elements in $\boldsymbol{F}_{i,j}$ is less than Δf_1, then only one of these elements is retained in $\boldsymbol{F}_{i,j}$. Also, refer to the original line spectrum sequence $\boldsymbol{F}_m$. If there are similar line spectra f_x to these k elements in $\boldsymbol{F}_m$, then retain the line spectrum closest to the original line spectrum among these k elements. If there are no similar line spectra to these k elements in $\boldsymbol{F}_m$, then retain the average frequency of these k elements. Additionally, the quality factor α of the retained element is k. If there are no similar elements, then $k = 1$. This results in a new difference frequency array F_n, which contains N difference frequencies.

Step 2: Calculate the minimum integer multiple distance between each line spectrum in set $\boldsymbol{F}_m$ and each element in the difference frequency array F_n to obtain $min |F_m(p) - \lambda F_n(q)|$, $\lambda = 1, 2, ..., +\infty$, $p = 1, 2, ..., M$, $q = 1, 2, ..., N$. If the minimum distance is less than Δf_2, the element in F_n is considered divisible, and its quality factor β is incremented by 1. The threshold Δf_2 is set as $\Delta f_2 = 1/f'_n$ when the element f'_n in F_n is less than or equal to 10 Hz, and remains $\Delta f_2 = 2/f'_n$ when f'_n is greater than 10 Hz.

Step 3: The quality factor δ corresponding to each difference frequency element in the difference frequency array F_n is given by $\delta = \alpha\beta.\delta$ integrates the repeatability α and divisibility β of difference frequencies, reflecting their possibility as shaft frequencies. For example, in $\delta = \alpha\beta$, α represents the occurrence frequency of difference frequencies in the original line spectrum, and β denotes the number of line spectrum frequencies divisible by the difference frequency. The difference frequency corresponding to the maximum quality factor δ is identified as the fundamental frequency. When different difference frequencies have the same quality factor δ, the difference frequency with the largest β is selected. If β is also the same, then check if they have a harmonic relationship. If they do, the lower frequency is taken as the fundamental frequency; otherwise, the higher frequency is taken as the fundamental frequency.

Utilizing shaft frequency information of ship targets as a criterion for fusion offers multifaceted advantages. Shaft frequency information is an intrinsic characteristic of ship targets, closely related to the structure and operational status of the vessels, and exhibits high stability and specificity. Different types of ships have distinct shaft system structures and operational parameters, leading to variations in shaft frequency information, which makes it a crucial basis for distinguishing between different ship targets.

If a particular shaft frequency is detected in the acoustic signal and the same shaft frequency is also detected in the magnetic signal, this significantly increases the confidence in identifying the target as a ship. In the natural environment, the probability of the simultaneous occurrence of acoustic and magnetic signals with the same frequency is extremely low. However, due to their specific operational mechanisms, ship targets generate acoustic and magnetic signals with identical shaft frequency characteristics. This fusion criterion based on shaft frequency information can effectively reduce the false alarm rate and enhance the detection and identification capabilities for underwater small targets.

Verification with sea trial data

To verify the correlation between the shaft-rate frequency acoustic field and the magnetic field, and to validate the effectiveness and accuracy of the target detection method that integrates acoustic and magnetic fields in a real marine environment, as well as the advantages of the fusion algorithm over a single physical field in extracting axis-frequency features, a bottom-mounted data acquisition platform was deployed in a port within a certain sea area of the East China Sea, the water depth in the port waters is 14 m. The average dissolved oxygen content in seawater is 5.66 ml/L, the average pH value of seawater is 8.14, and the average salinity of the seawater surface layer is 30.72‰ at the bottom. Due to the busy shipping within the port, acoustic interference and electromagnetic power frequency interference noise are relatively high (while acoustic and electromagnetic noise in the far-deep sea areas are relatively low). The underwater acoustic and magnetic data of medium and large vessels measured within the port were used for validation. The bottom-mounted measurement platform is shown in Fig. 3. The acoustic field acquisition device is a scalar acoustic sensor with a sampling rate of 8,000 Hz, and the magnetic field acquisition device is a fluxgate sensor with a sampling rate of 400 Hz.

Analysis of the correlation between shaft-rate acoustic field and shaft-rate magnetic field

The bottom-mounted detection platform was deployed within the port's navigation channel, where a substantial number of vessels frequently enter and exit the port. This high traffic volume ensures a rich dataset for analysis. Data from selected vessels were analyzed to provide insights into the characteristics of the acoustic and magnetic fields. Figures 4 and 6 present the raw time-domain data of the acoustic and magnetic fields for Ships A and B, respectively, as they passed through the channel. Following the methods described earlier, line spectra were extracted from the acoustic and magnetic fields, and the extracted line spectra were purified to produce the line spectrum plots shown in Figs. 5 and 7.

As shown in Fig. 4, there is no obvious correlation between the acoustic and magnetic fields in the raw time-domain data of Ship A. The time-domain plot of the acoustic field exhibits distinct pass-by characteristics, while the magnetic field data lack clear target features. Analysis of Fig. 5 reveals that the line spectra of the shaft-rate acoustic field and the shaft-rate magnetic field exhibit a certain degree of frequency correspondence. Specifically, the line spectra overlap at 4.49Hz, 8.98Hz, 11.13 Hz, 13.67Hz, 21.48 Hz, 32.81 Hz, 38.05 Hz, with additional line spectra appearing at other frequencies that are close in value. Upon further examination, it is evident that both the shaft-rate acoustic and magnetic fields are based on the propeller rotation frequency and are closely related to the blade rate and its harmonics. The measured shaft rate of the vessel is 4.49 Hz, with 8.98 Hz and 13.67 Hz corresponding to its multiples and harmonic-related signals.

As shown in Fig. 6, in the raw time-domain data of Ship 'B', there is also no obvious correlation between the acoustic and magnetic fields. However, both the acoustic and magnetic fields exhibit distinct pass-by characteristics. Analysis of Fig. 7 reveals that the line spectra of the shaft-rate acoustic field and the shaft-rate magnetic field show a certain degree of frequency correspondence. Specifically, the line spectra overlap at 9.57 Hz, 19.13 Hz, 24.60 Hz, and 39.06 Hz. Additionally, line spectra with similar frequencies are observed at other frequency points.

Through the above analysis, it can be seen that different types of ships show no obvious corresponding relationship in the time-domain waveforms of acoustic and magnetic fields. However, there is a good correspondence in the line spectra of shaft-frequency acoustic fields and shaft-frequency magnetic fields. Nevertheless, the line spectra of shaft-frequency acoustic and magnetic fields are not strictly corresponding. Analysis shows that this is because the acoustic and magnetic fields are affected by environmental noise, ship motion noise, etc., during the ship's operation, leading to phenomena such as line spectra being submerged by noise and frequency drift (typically < 1 Hz). However, the real line spectrum frequencies of the same target should exhibit clustered distribution around the shaft frequency/blade frequency. The shaft frequency signal is generated by propeller rotation, and the shaft frequency of medium to large ships generally ranges from 1 to 7 Hz (corresponding to propeller speeds of about 60 to 420 revolutions per minute). A 1 Hz threshold covers

(a) Submerged acoustic and magnetic detection platform

(b) Layout diagram of detection platform

Fig. 3. Submerged detection platform and layout diagram.

the reasonable range of shaft frequency and its fundamental frequency fluctuations, which can avoid misjudging multi-path interference spectral lines of the same frequency as different features. Therefore, the correlation between the shaft-frequency acoustic field and shaft-frequency magnetic field of the same ship can serve as an important basis for target judgment.

Shaft-rate feature extraction by fusing shaft-rate acoustic field and shaft-rate magnetic field

To validate the effectiveness of the line-spectrum fusion algorithm compared with the shaft-rate line-spectrum feature extraction using a single physical field, data from the shaft-rate acoustic field and shaft-rate magnetic field of multiple vessels were utilized for verification. To ensure comparability of the extracted shaft-rate features, the same parameters were employed for feature extraction in both single physical field and fused physical field scenarios. The data selected for analysis were from Cargo Ships A and B, with specific analyses presented in Figs. 8 and 9.

Analysis of the shaft-rate acoustic field, shaft-rate magnetic field, and the fused shaft-rate line-spectrum signals for Ship A reveals that the number of line spectra extracted from a single acoustic field is greater than that from a single magnetic field. This difference is determined by the signal-to-noise ratio (SNR) of the respective physical fields. To enhance the reliability of the extracted line spectra, the line-spectrum extraction method proposed in Section"Shaft-rate frequency feature extraction method integrating acoustic field and magnetic field"incorporates both sliding and fixed thresholds. When the SNR is low, the number of extracted line spectra decreases. However, as shown in Fig. 7, even with a smaller number of corresponding spectra, there remains a clear correlation between the frequencies.

Figure 9 presents the shaft-rate line-spectrum signals extracted from the acoustic field, magnetic field, and the fused acoustic-magnetic field for Medium-sized Cargo Ship B. It is evident that the number of line spectra extracted from a single acoustic field is greater than that from a single magnetic field. However, after fusing the line spectra of the acoustic and magnetic fields, the number of extracted line spectra is significantly increased, which notably mitigates the impact of line-spectrum loss. Moreover, the shaft-rate line spectra and their harmonics extracted from the fused acoustic and magnetic fields are more abundant and can serve as an important basis for target identification.
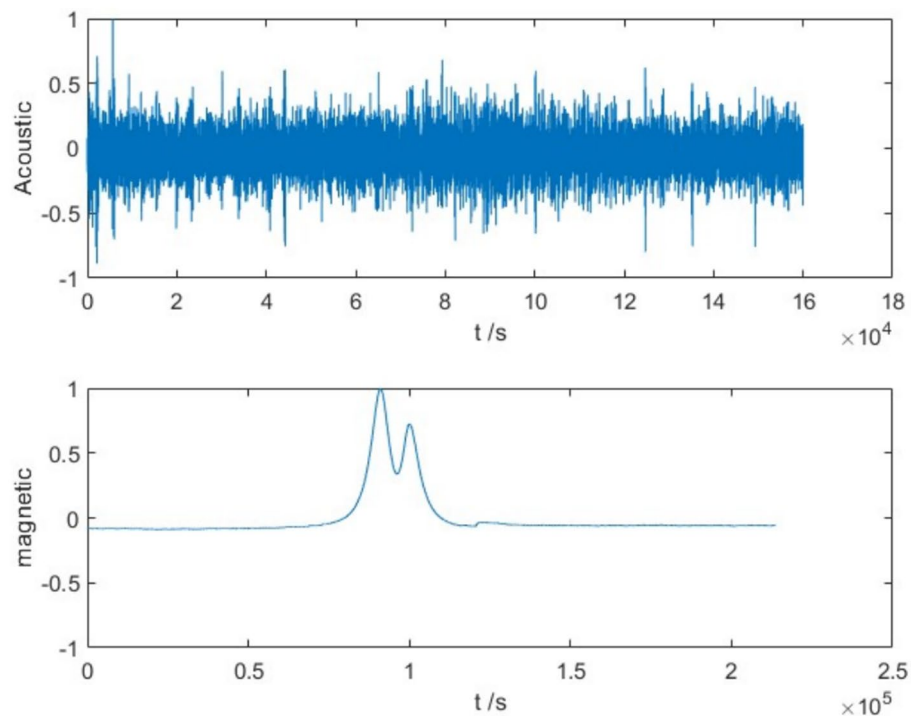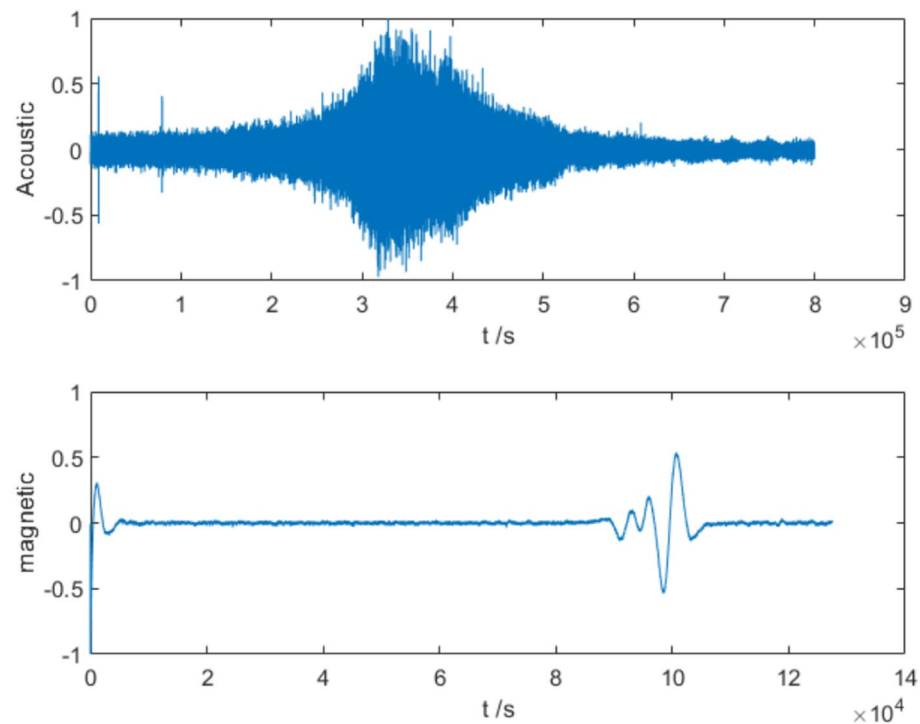
Fig. 4. Time domain diagram of Ship A acoustic and magnetic data.
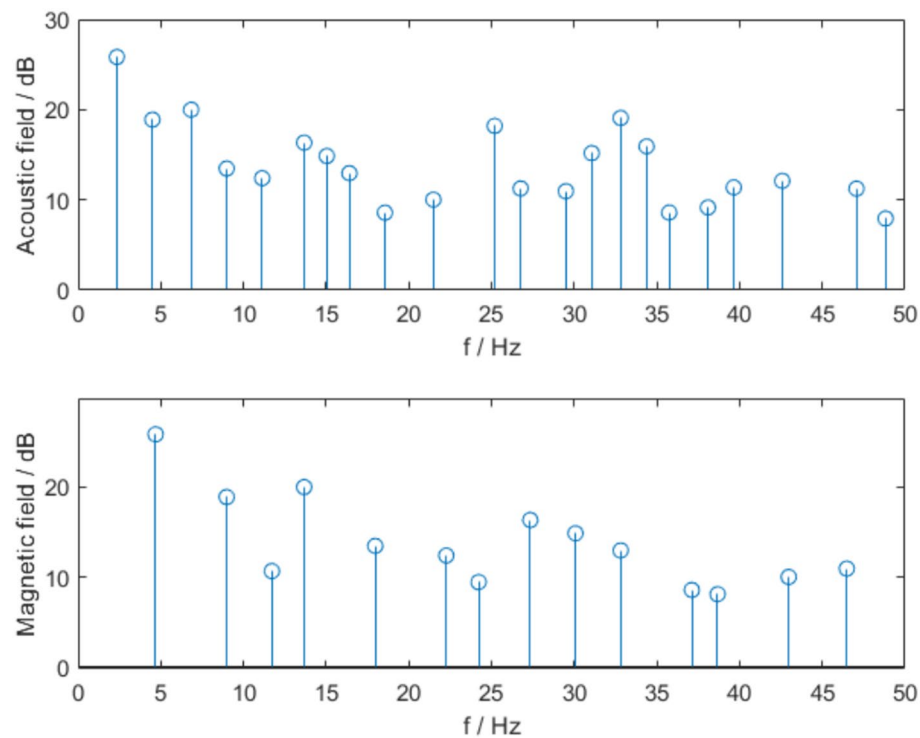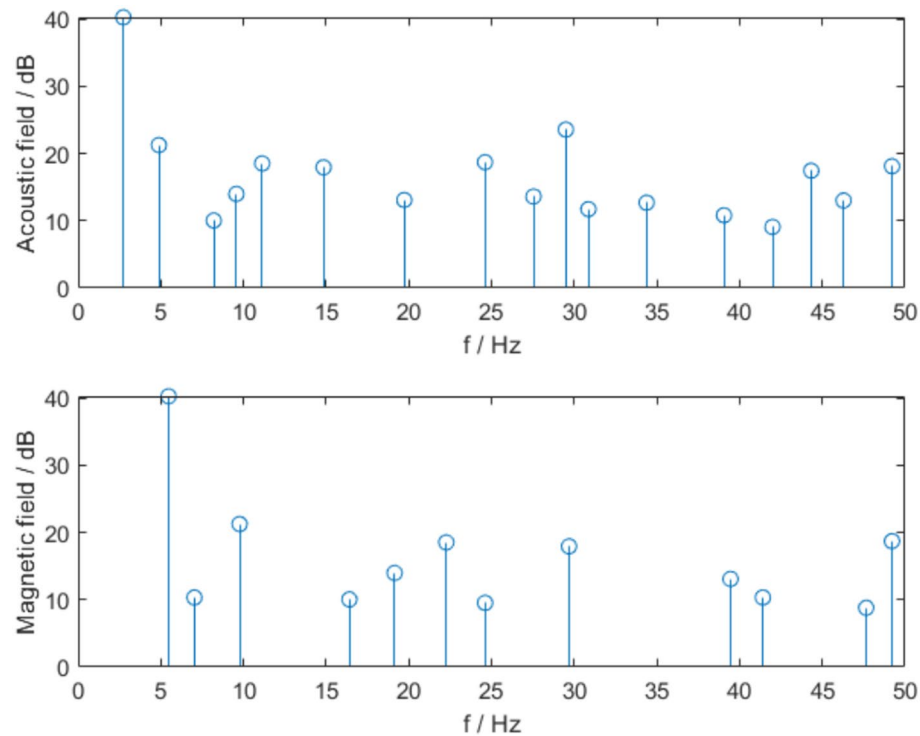

Fig. 5. Shaft rate acoustic field and axis frequency magnetic field line spectrum of Ship A.

To validate the advantages of the acoustic-magnetic fusion method for extracting shaft-rate features compared to detection using a single physical field, the sliding window method was employed to extract the fundamental frequency. Within a specified time interval, the estimation of the vessel's shaft rate across the entire interval was evaluated. The shaft-rate data from Ships A and B were used for extraction, and the figures display only the

Fig. 6. Time domain diagram of Ship B acoustic and magnetic data.

Fig. 7. Shaft rate acoustic field and axis frequency magnetic field line spectrum of Ship B.

frequencies corresponding to the maximum quality factor. The results are shown in Figs. 10 and 11, where the color indicates the quality factor of the shaft-rate data.

Analysis of Figs. 10 and 11 reveals that within the passage interval, the shaft-rate values extracted from the single acoustic field and single magnetic field exhibit fluctuations. The fluctuations in the magnetic field shaft rate
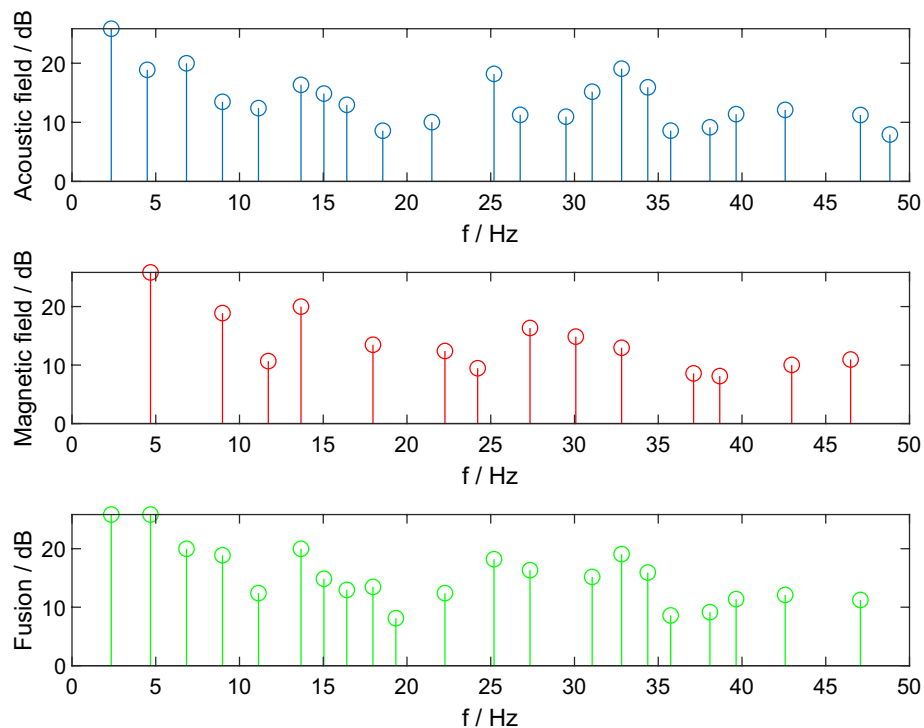
Fig. 8. Acoustic, magnetic field and their fused shaft-rate line spectrum of one middle sized cargo Ship A.
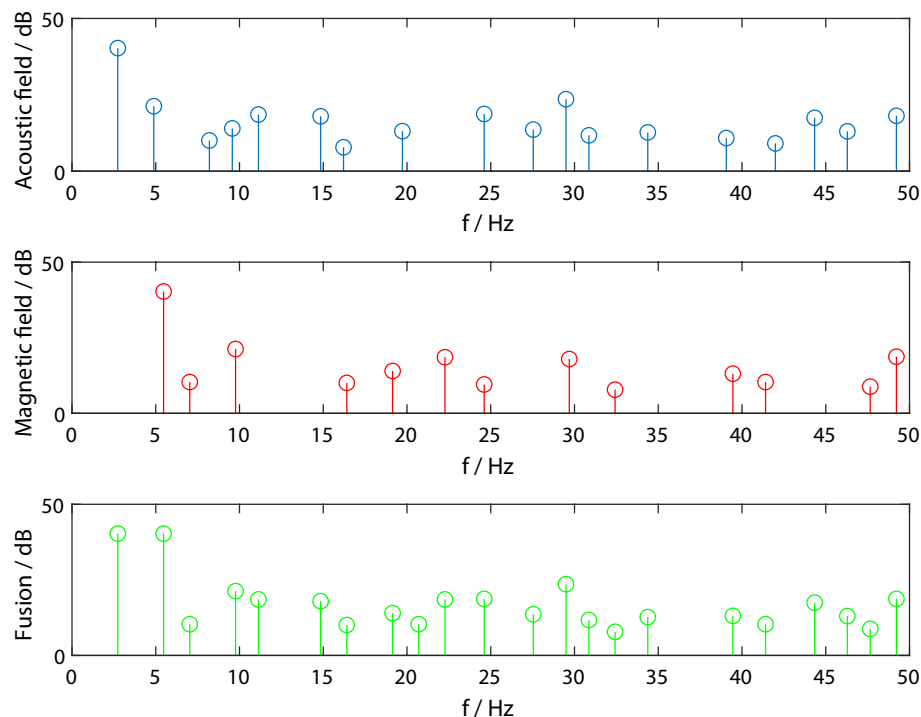

Fig. 9. Acoustic, magnetic field and their fused shaft-rate line spectrum of one middle sized cargo Ship B.

are more pronounced than those in the acoustic field, attributable to the differing signal-to-noise ratios (SNRs) of the acoustic and magnetic signals. In contrast, when the acoustic and magnetic data are fused, the extracted shaft rate is more stable compared to that obtained from a single physical field. For Cargo Ship A, the shaft rate remains consistently at 2.53 Hz, while for Cargo Ship B, it remains at 2.95 Hz. Moreover, throughout the entire passage interval, the fundamental frequency of the vessels remains essentially constant. The comparison
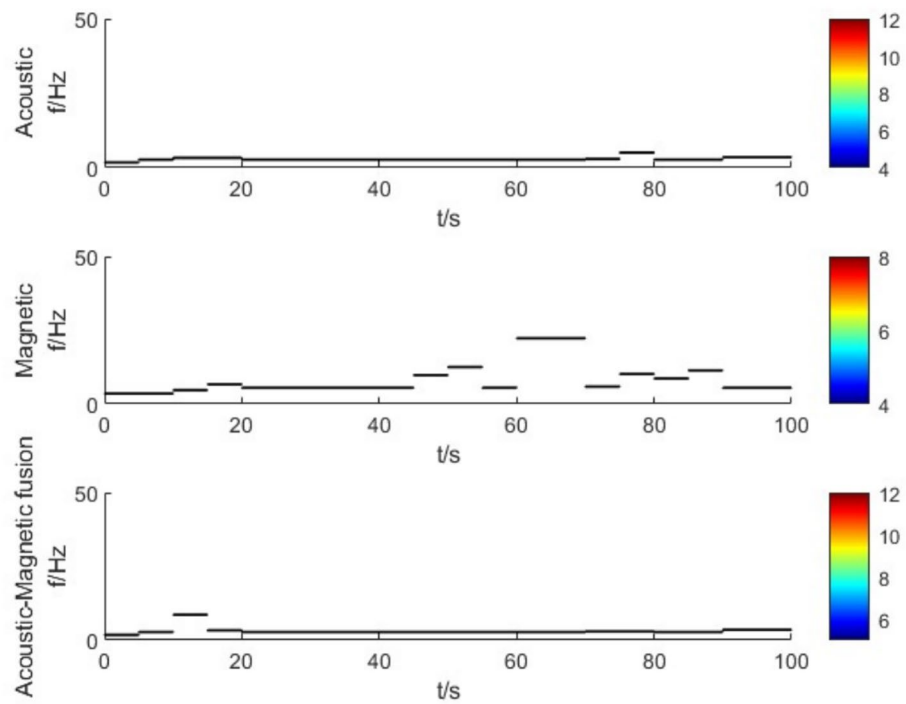
Fig. 10. Shaft-rate frequency estimation of medium passenger Ship A.
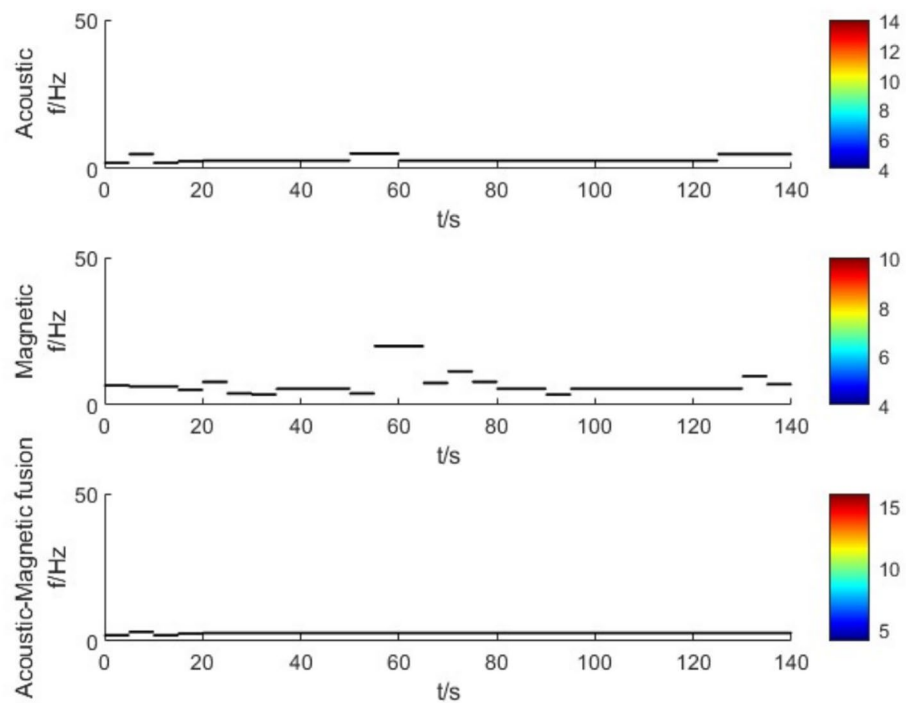
Fig. 11. Shaft-rate frequency estimation of medium passenger Ship B.

demonstrates that the shaft-rate estimation achieved through fusion is significantly superior to that obtained using a single physical field.

This approach is consistent with the study's objective of showcasing the complementary characteristics of acoustic and magnetic fields. Specifically, the figures effectively demonstrate that:

Single magnetic field estimations exhibit more pronounced volatility (likely due to environmental magnetic interferences), while single acoustic field results are affected by multipath effects;

The fused method integrates dual-field information, significantly stabilizing the shaft-rate estimation and aligning with the theoretical expectation of error cancellation.

Conclusion

The manuscript pioneers the fusion of shaft-rate acoustic fields and shaft-rate magnetic fields for extracting the shaft-rate features of vessels. It begins by introducing distinct line-spectrum extraction methods for shaft-rate acoustic and magnetic fields. Subsequently, a method for fusing and purifying the line spectra of acoustic and magnetic fields is proposed, followed by the extraction of shaft-rate features based on the greatest common divisor (GCD) method. Finally, the proposed method is validated using real-measurement data from multiple vessels. The results demonstrate that:

(1) Frequency correspondence of acoustic-magnetic line spectra.

The line spectra of shaft-rate acoustic and magnetic fields from the same target exhibit significant frequency correspondence.

Ship A shows overlapping line spectra at 4.49 Hz, 8.98 Hz (2×4.49 Hz), and 13.67 Hz (3×4.49 Hz) (shown in Fig. 5);

Ship B demonstrates consistent frequencies at 9.57 Hz, 19.13 Hz (2×9.57 Hz), and 39.06 Hz (4×9.57 Hz) (shown in Fig. 7), verifying the integer multiple relationship between shaft frequency and blade passing frequency.

(2) Mitigation of line-spectrum loss and estimation accuracy enhancement via fusion.

Line-spectrum quantity: For Cargo Ship A, the single acoustic field extracts 7 line spectra, the single magnetic field extracts 4, and the fused field extracts 10—an increase of 42.8% compared to the single acoustic field (shown in Fig. 8);

Estimation stability: The shaft-rate estimation via the fusion method shows significantly reduced fluctuations. For instance, the fused estimation of Ship A remains stable at 2.53 Hz, while the single magnetic field fluctuates by ± 0.8 Hz; the fused estimation of Ship B stabilizes at 2.95 Hz, whereas the single acoustic field fluctuates by ± 0.5 Hz (shown in Figs. 10 and 11).

(3) Superiority of fusion method over single-field detection.

Correct identification rate: Validation across multiple vessels shows that the fusion method achieves a correct identification rate of over 90% for shaft frequency, compared to approximately 75% for the single acoustic field and 60% for the single magnetic field;

Noise resistance: The number of pseudo-peaks in the fused line spectra is reduced by approximately 30% compared to single fields (e.g., the fused spectrum of Ship B in Fig. 9).

In summary, using shaft-rate information as a fusion criterion effectively reduces the false alarm rate. The probability of coincident frequencies in natural acoustic and magnetic signals is < 1%, whereas ship targets exhibit consistent shaft frequencies in both fields, increasing target identification confidence by over 95%.

Data availability

The data presented in this study are available upon request from the corresponding author.

References

1. Tu, H. W. et al. A novel algorithm to solve for an underwater line source sound field based on coupled modes and a spectral method. *J. Comput. Phys.* **468**, 111478 (2022).
2. Nicholas, M., Haidy, E. & Donald, M. Using feature extraction to perform equipment health monitoring on ship-radiated noise. *Acoustics* **5**(4), 1180–1193 (2023).
3. Ye, W. et al. Ship shaft-rate electric field signal denoising method based on VMD-MSS. *J. Marine Sci. Eng.* **12**(4), 544 (2024).
4. Park, J., Seok, J. & Hong, J. Autoencoder-based signal modulation and demodulation methods for sonobuoy signal transmission and reception. *Sensors* **22**(17), 6510–6510 (2022).
5. Li, M. H. et al. Simulative evaluation of the underwater geodetic network configuration on kinematic positioning performance. *Remote Sens.* **14**(8), 1939–1939 (2022).
6. Qarabaqi, P. & Stojanovic, M. Statistical characterization and computationally efficient modeling of a class of underwater acoustic communication channels. *IEEE J. Ocean. Eng.: J. Devot. Appl. Electr. Electron. Eng. Ocean. Environ.* **38**(4), 701–717 (2013).
7. Liu, X. Y., Zhou, H., Ge, X. Y. & Jiao, H. F. Development of Underwater Wireless Communication Equipment Technology. *Strategic Study CAE* **26**(2), 38–49. https://doi.org/10.15302/J-SSCAE-2024.02.006 (2024).
8. Stojanovic, M. & Preisig, J. Underwater acoustic communication channels: Propagation models and statistical characterization. *IEEE Commun. Mag.: Articles, News, Events Interest Commun. Eng.* **47**(1), 84–89 (2009).
9. Finn, B. J. et al. *Computational Ocean Acoustics* 32–48 Springer(2011).
10. Chen, Y., Luo, Y. G. & Li, J. Research on Application of Underwater Object Detection Based on Multimodal Perception. *Digit. Ocean Underw. Warf.* **7**(3), 334–341 (2024) (**in Chinese**).
11. Wang, Z., Qiu, J., Xie, D., Ou, J. & Xu, Q. Weak magnetic anomaly signal detection based on the entropy of mixed differential signal. *AIP Adv.* **11**(1), 015013 (2021).
12. Liu, Y. F., Zhang, N., Shi, Z. S. & Gu, H. C. Research on a matching detection method for magnetic anomaly of underwater targets. *AIP Adv.* **13**(2), 025248 (2023).
13. Nie, X. et al. Energy detection based on undecimated discrete wavelet transform and its application in magnetic anomaly detection. *PLoS ONE* **9**(10), e110829. https://doi.org/10.1371/journal.pone.0110829 (2014).
14. Shen, Y., Wang, J. & Gao, J. Q. Noise Suppression for Vector Magnetic Anomaly Detection by Noise Spatial Characteristics Investigation. *IEEE Geosci. Remote Sens. Lett.* **19**, 1–4 (2022).

15. Bronner, A. et al. Magnetic signature of large exhumed mantle domains of the Southwest Indian Ridge – results from a deep-tow geophysical survey over 0 to 11 Ma old seafloor. *Solid Earth* **5**(1), 339–354 (2014).
16. Keller, B. A. et al. Map-Like Use of Earth'S Magnetic Field in Sharks. *Curr. Biol.* **31**(13), 2881–2886 (2021).
17. Zhang, Y. H. et al. A review of underwater acoustic target detection and recognition technology based on information fusion. *J. Signal Process.* **39**(10), 1711–1727 (2023).
18. Sun, H. X., Wang, Z., Lan, T., Zhang, S. Y. & Qiu, J. Adaptive cascade detection of weak magnetic anomalies based on marine predators algorithm-stochastic resonance. *AIP Adv.* **13**(2), 025147 (2023).
19. Han, C. *Multi-Source Information Fusion* (Tsinghua University Press, 2010).
20. Yang, W. *Multi-sensor Data Fusion and Its Applications* (Xidian University Press, 2004).
21. Zhao, Z. G., Xiong, Z. H. & Wang, K. *Conceptions, Methods and Applications on Information Fusion* (National Defense Industry Press, 2012).
22. Pan, Q. et al. *Multi-source Information Fusion Theory and its Applications* (Tsinghua University Press, 2013).
23. Song, M., Gong, S. G., Zhou, J. & Lu, X. C. Calculation of the Electric Field Generated by Vessel Moving Across Geomagnetic Field in Seawater. *Acta Electron. Sin.* **03**, 464–467 (2003) (**(in chinese)**).
24. Cheng, J. F., Yu, P., Zhang, J. W. & Xie, T. T. Application and development of underwater electric field detection and location technology. *J. Nav. Univ. Eng.* **34**(4), 68–74. https://doi.org/10.7495/j.issn.1009-3486.2022.04.012.(inchinese) (2022).
25. Bostick, F., Smith, H. & Boehl, J. *The detection of ULF-ELF emissions from moving ships[R]* 13–24 (State Academic Educational Institutions, 1977).
26. Zolotarevskii, Y. et al. Methods of measuring the low-frequency electric and magnetic fields of ships. *Meas. Tech.* **48**(11), 1140–1144 (2005).
27. Ma, C. et al. Elucidating the Synergic Effect in Nanoscale MoS2/TiO2 Hetero interface for Na-Ion Storage. *Adv. Sci.* **9**, 2204837 (2022).
28. Cheng, J. F., Zhang, J. W., Jiang, Y. X. & Yu, P. Development Status of Underwater Electromagnetic Detection Technology. *Digit. Ocean & underw. Warf.* **04**, 45–49 (2019) (**(in chinese)**).
29. Chen, D. et al. Natural disaster monitoring with wireless sensor networks: A case study of data-intensive applications upon low-cost scalable systems. *Mobile Netw. Appl.* **18**, 651–663 (2013).
30. Corke, P. et al. Environmental wireless sensor networks. *Proc. IEEE* **98**, 1903–1917 (2010).
31. Xu, W. et al. Marine information gathering, transmission, processing, and fusion: Current status and future trends. *Sci. Sinica Inform.* **46**(08), 1053–1085 (2016).
32. Wang, Y. et al. Ship Shaft-Rate Electric Field Signal Denoising Method Based on VMD-MSS. *J. Marine Sci. Eng.* **12**(4), 544 (2024).
33. Chen, Y., Luo, Y. H. & Li, J. Research on Application of Underwater Object Detection Based on Multimodal Perception. *Digit. Ocean & Underw. Warf.* **7**(3), 334–341. https://doi.org/10.19838/j.issn.2096-5753.2024.03.012 (2024) (**(in chinese)**).
34. Yu, P., Cheng, J. F. & Zhang, J. W. Ship Target Tracking Using Underwater Electric Field. *Progress Electromagn. Res. M* **86**, 49–57. https://doi.org/10.2528/PIERM19052001 (2019).
35. Jiang, Z. K. Research on Underwater Target Multi-physical Field Coupling Detection Method[D]. *Harbin Eng. Univ.* https://doi.org/10.27060/d.cnki.ghbcu.2022.000544 (2022).
36. Wang, X., Wang, S., Hu, Y. & Tong, Y. Mixed Electric Field of Multi-Shaft Ship Based on Oxygen Mass Transfer Process under Turbulent Conditions. *Electronics* **11**(22), 3684. https://doi.org/10.3390/electronics11223684 (2022).
37. Wang, F. et al. Underwater object detection by fusing features from different representations of sonar data. *Front. Inform. Technol. Electr. Eng.* **24**(6), 828–843. https://doi.org/10.1631/FITEE.2200429 (2023).
38. He, Z. Y. & Zhang, Y. P. Modeling and simulation research of ship-radiated noise. *Noise control* **12**, 52–55 (2005) (**(in chinese)**).
39. Xu, Z. H., Li, Y. G. & Luo, M. Seabed survey and property analysis of ship's shaft-rate electromagnetic signal. *J. Harbin Eng. Univ.* **39**(4), 652–657. https://doi.org/10.11990/jheu.201612066.(inchinese) (2018).
40. Jiang, R. X., Li, G. D. & Liu, Q. Shaft-rate magnetic field modeling method from magnetic axis rotation. *J. Naval Univ. Eng.* **36**(1), 94–99. https://doi.org/10.7495/j.issn.1009-3486.2024.01.015 (2024).
41. Yue, R. Y., Tian, Z. X., Lv, J. J. & Zhang, Y. H. Study on attenuation law of the vessel's shaft rate electric field based on the time harmonic electric dipole model. *Ship Sci. Technol.* **31**(10), 21–25 (2009).
42. Zhang, S. N. & He, Z. X. Research on Amplitude Characteristics of Target Axial-frequency Electromagnetic Field Based on Undersea Detection. *Digit. Ocean Underw. Warf.* **6**(05), 583–594. https://doi.org/10.19838/j.issn.2096-5753.2023.05.008 (2023).
43. Han, D. F. et al. Adaptive maximum generalized Gaussian cyclostationarity blind deconvolution for the early fault diagnosis of high-speed train bearings under non-Gaussian noise. *Adv. Eng. Inform.* **62**, 102731–102731 (2024).
44. Han, D. F. et al. Dynamic detection mechanism model of acoustic emission for high-speed train axle box bearings with local defects. *Mech. Syst. Signal Process.* **235**, 112943–112943 (2025).

Author contributions

Conceptualization, Peng Yu and Jiawei Zhang; Data curation, Taotao Xie, Peng Yu and Jiawei Zhang; Formal analysis, Taotao Xie, Qing Ji and Peng Yu; Investigation, Qing Ji and Jiawei Zhang; Methodology, Taotao Xie, Qing Ji and Peng Yu; Resources, Qing Ji, Peng Yu and Jiawei Zhang; Software, Taotao Xie and Qing Ji; Validation, Taotao Xie; Writing – original draft, Taotao Xie and Qing Ji; Writing – review & editing, Taotao Xie and Jiawei Zhang.

Funding

Declarations

Competing interests

The authors declare no competing interests.

Additional information

Correspondence and requests for materials should be addressed to Q.J. or P.Y.

Reprints and permissions information is available at www.nature.com/reprints.

Publisher's note Springer Nature remains neutral with regard to jurisdictional claims in published maps and institutional affiliations.